

Calculating or simulating the dose rate? A comparison

Michael Discher¹, Barbara Mauz^{1,2}, Loïc Martin³, Julie A. Durcan⁴, Georgina E. King⁵, Evangelos Tsakalos⁶, John Christodoulakis⁶ and Andreas Lang¹

¹Department of Geography and Geology, University of Salzburg, Salzburg, Austria

²School of Environmental Sciences, University of Liverpool, Liverpool, United Kingdom

³Institut de Recherche sur les Archéomatériaux, UMR 5060 CNRS, Centre de Recherche en Physique Appliquée à l'Archéologie (CRP2A), Maison de l'archéologie, Université Bordeaux Montaigne, Pessac Cedex, France

⁴School of Geography and the Environment, University of Oxford, Oxford, United Kingdom

⁵Institute of Earth Surface Dynamics, University of Lausanne, Switzerland

⁶Laboratory of Archaeometry, Institute of Nanoscience and Nanotechnology (INN), National Centre for Scientific Research, N.C.S.R. 'Demokritos', Athens, Greece

Highlights:

Dose rates from sedimentary and archaeological samples were determined using two approaches

Three commonly used dose-rate calculators were employed, as well as Monte Carlo simulation using DosiVox

Dose rates are consistent within uncertainties confirming robustness of the commonly used approach but calculated uncertainties vary between techniques

Monte Carlo simulations reveal the impact of heterogeneous sedimentary environment on the dose-rate accuracy

Keywords:

Dose-rate calculators, Monte Carlo simulations, luminescence dating

Abstract

Accurate determination of the environmental radiation dose-rate is crucial for dosimetric dating methods. Two approaches for dose-rate estimation are currently employed: (1) calculating and summing up individual dose-rate components, including propagation of uncertainties and (2) simulating the radiation field and calculating the absorbed dose using a Monte Carlo approach.

Here we compare dose-rate estimation using the two aforementioned approaches, applied to six sedimentary quartz samples with differing radionuclide concentrations, chemical composition, grain-size distribution and water content and to one heterogeneous archaeological sample. For approach (1) two web-based, freely accessible calculators, "Dose-Rate calculator" (DRc), "Dose Rate and Age Calculator" (DRAC) and a bespoke spreadsheet were used. For approach (2) DosiVox, a Geant4 Monte Carlo simulation toolkit was employed which allows the definition of material properties such as chemical composition, density and porosity in addition to radionuclide concentrations and water

content in a three dimensional geometry. The sensitivity of dose rate to material properties, usually assumed to be constant over the burial time scale, was also tested. The results obtained using the three dose-rate calculators for sedimentary quartz samples are consistent within uncertainties, mainly because the conversion and correction factors are all taken from the same references. Comparing these results with those obtained from DosiVox simulations show grain-size dependent dose-rate differences, caused by the charge build-up and attenuation of the irradiated grain-size fraction. Moreover, it reveals that the effect of porosity and moisture on dose rate is grain-size dependent. For the heterogeneous archaeological sample the total dose rate determined by a calculator is inaccurate for the alpha- and too precise for the beta dose-rate. We conclude that the standard approach to dose-rate estimation is robust and that DosiVox is an important diagnostic tool for samples originating from complex environments.

1. Introduction

In trapped charge dating the accurate determination of the environmental radiation dose-rate is crucial because it constitutes the denominator of the age equation. Typically, the dose rate of a sample is calculated based on the concentration of radionuclides and on a number of well-established factors for energy attenuation and absorption (e.g. Brennan et al., 1991; Mejdahl, 1979; Guérin et al., 2012) and for energy to dose conversion (Adamiec and Aitken, 1998; Liritzis et al., 2013; Guérin et al., 2011a). Besides standard calculation methods, as recently outlined by Durcan et al. (2015), numerical (Monte Carlo) modelling can be employed, particularly in cases where basic assumptions such as homogeneous radionuclide distributions or constant pore filling during the burial period by water, air, carbonate or other materials are not fulfilled (Nathan and Mauz, 2008; Guérin and Mercier, 2012).

In this paper, we compare the performance of two commonly used dose-rate calculators, a bespoke spreadsheet and a Monte Carlo simulator applied to six samples. These samples differ in (i) composition (especially quartz concentrations), (ii) bulk density and porosity, and (iii) grain-size distribution, in order to cover a wide range of environmental configurations. In addition, a sample from a non-homogeneous setting was used. The study allows us to identify key parameters contributing to inaccuracies in dose-rate estimates when standard dose-rate calculation for variable geometries of quartz grain-packing and matrix chemical composition is employed.

2. Materials and Methods

82 Six of the samples used in this study were selected from the archive of the Luminescence
 83 Dating Laboratory, University of Liverpool (denoted LV samples). They cover a range of
 84 depositional environments and radionuclide concentrations (U, Th, K), chemical
 85 composition, grain-size distribution and pore filling (Table 1). To test calculator
 86 performance in non-homogeneous settings a sample from the archaeological site “Mas
 87 d’Azil” (Martin et al., 2015b) was also included. The latter sample is composed of a
 88 succession of millimeter-thick layers which vary in terms of mineral composition, grain
 89 size and radioactivity. The average values of this sample calculated across all layers are
 90 listed in Table 1 and details for individual layers are provided in the supplementary
 91 information (Table S1). The dose rates of all samples were determined using two
 92 approaches: (1) calculating individual dose-rate components and summing them to
 93 produce the total dose-rate using freely accessible web-based dose-rate calculators
 94 (DRAC, DRc) and a bespoke spreadsheet; (2) simulating the radiation field and
 95 calculating the total absorbed dose using Monte Carlo modelling (DosiVox). Both
 96 approaches are based on the infinite-matrix assumption (Roesch and Attix, 1968; Aitken,
 97 1985) and all sample data in both approaches were processed using the energy dose
 98 conversion factors of Guérin et al. (2011a), the alpha attenuation factors of Brennan et al.
 99 (1991) and the beta attenuation factors of Guérin et al. (2012). For Monte Carlo
 100 modelling, quartz-grain distributions were simulated following the SiO₂ content, the
 101 porosity and the grain-size distribution of the relevant sample where grain-size
 102 distribution stands for the mean of the grain-size class of Wentworth (1922). Porosity was
 103 calculated using the median diameter of the sample’s grains following the approach of
 104 Wu and Wang (2006). Grain-size data of all LV samples are listed in Table S2. Details of
 105 uncertainty calculation are provided in the relevant sections (see below) and discussed in
 106 section 3.3.

108 **2.1 DRAC**

109 Dose Rate and Age Calculator (DRAC; Durcan et al., 2015) is an open-access, web-based
 110 program for dose-rate and age calculation in trapped charge dating. It can be accessed at
 111 <http://www.aber.ac.uk/alrl/drac> or used within the R Luminescence package (Kreutzer et
 112 al., 2017). The program code is available at
 113 <https://github.com/DRAC-calculator/DRACcalculator>. In DRAC, alpha, beta and gamma
 114 dose-rates (and uncertainties) are either provided by the user or calculated from user
 115 provided radionuclide concentrations and user-selected published conversion factor
 116 datasets (Liritzis et al., 2013; Guerin et al., 2011a; Adamiec and Aitken, 1998). Dose-

178
179
180
181 117 rates are then corrected for attenuation, absorption, chemical etching, alpha efficiency and
182 118 moisture content (Durcan et al., 2015 and references therein). The majority of the
183 119 correction factors are user-defined or user-specified. The total environmental dose-rate is
184 120 calculated by combining internal (alpha and beta) and external (alpha, beta, gamma and
185 121 cosmic) dose rates. Details of these datasets and calculations including calculation of the
186 122 uncertainties are given in Durcan et al. (2015) and in the accompanying supplementary
187 123 information.

191 124 192 125 **2.2 DRc**

193 126 Dose-Rate calculator, DRc (Tsakalos et al., 2016) is a Java-based software for dose-rate
194 127 and age calculation for dosimetric dating. It is freely accessible at
195 128 <http://www.ims.demokritos.gr/download/DRcalculator.exe>. It calculates the alpha, beta
196 129 and gamma dose-rates (and uncertainties) from radionuclide concentrations provided by
197 130 the user, and employs the conversion factors of Guérin et al. (2011a). It corrects for
198 131 attenuation and absorption following Guérin et al. (2012), Readhead (2002a, b) and
199 132 Brennan et al. (1991), for chemical etching following Brennan (2003) and Bell (1979),
200 133 for alpha efficiency following Bell (1979) and for moisture content following Guérin and
201 134 Mercier (2012), Nathan and Mauz, (2008) and Aitken (1985). The total environmental
202 135 dose rate is calculated by combining internal (alpha and beta) and external (alpha, beta,
203 136 gamma and cosmic) dose rates with uncertainties calculated and propagated in quadrature
204 137 at each stage of the calculation process. Details of DRc, including calculation of the
205 138 uncertainties are given in Tsakalos et al. (2016).

213 139 214 140 **2.3 Bespoke spreadsheet template**

215 141 Our spreadsheet-based calculator was first established by Lang et al. (1996) and was then
216 142 continuously updated with the latest published conversion and attenuation factors (e.g.,
217 143 Guerin et al., 2011). The spreadsheet calculates the alpha, beta and gamma dose-rate
218 144 components from radionuclide concentrations, corrects these as required for absorption
219 145 and attenuation using factors presented by Mejdahl (1979), Guérin and Mercier (2012),
220 146 Nathan and Mauz (2008) and Guérin et al. (2011a) and sums these values to estimate the
221 147 total dose-rate. Uncertainties are determined at each stage of the calculation process and
222 148 the total uncertainty is the sum of all errors as calculated by Gaussian error propagation
223 149 assuming normally distributed errors.

228 150 229 230 151 **2.4 DosiVox**

DosiVox (Martin et al., 2015a) uses the Geant4 Monte Carlo simulation toolkit. It models random packing of spheres in a sedimentary matrix in different 3D geometries: cube, cylinder or voxel subdivided in smaller voxels. It simulates the radiation field for a given geometry according to the user-defined input of (1) source of radioactivity (matrix or grain), (2) radionuclide concentration and (3) material properties: chemical composition, density, porosity. The software records the dose absorbed in individual grain-size fractions and simulates it as part of the total infinite matrix dose-rate. The size of the selected geometry depends on the number of grains simulated, where a reasonable quantity of grains results in the following dimensions of a cube, for example: 3 mm³ for alpha simulation (dose rate is recorded in a 0.5x0.5x0.5 mm³ central cube); 15 mm³ for beta simulation (dose rate is recorded in a 5x5x5 mm³ central cube); 0.9 m³ for gamma simulation (dose rate is recorded in a 0.15x0.15x30 cm³ column at the centre). The matrix composition and density are estimated by subtracting the mass of the quartz grains from the total mass. For energy to dose conversion, energy spectra are required besides factors. These were adopted from Guérin et al. (2011b) for beta emissions of the U-, Th-series and K and for gamma emissions of the U- and Th-series. For alpha- and for K-gamma emissions, the spectra were taken from ENSDF (Evaluated Nuclear Structure Data Files of the Brookhaven National) version Nov. 2012.

The statistical dispersion of the Monte-Carlo calculations is estimated as twice the standard deviation of the dose rate determined for a given geometry which, in turn, is derived from simulating U, Th and K contributions to the corresponding beta and gamma dose rates.

The uncertainty of the infinite matrix dose-rate ($\Delta\dot{D}_X$ in Gy/ka), as derived from the radionuclide concentration and statistical dispersion is calculated using:

$$\Delta\dot{D}_X = \sqrt{(Fc_X \cdot \Delta C_X)^2 + (2\sigma)^2} \quad (1)$$

where C_X is the concentrations of radioactive element X and Fc_X is the corresponding conversion factor; 2σ is the 2 sigma statistical dispersion of the dose rate. The values of $\Delta\dot{D}_X$ for U, Th and K contributions are then added linearly and combined with those originating from porosity and grain-size distribution:

$$\Delta\dot{D} = \dot{D} \cdot \sqrt{(\Delta\dot{D}_{K,U,Th}/\dot{D}_{inf})^2 + (\Delta\dot{D}_{moist}/\dot{D})^2 + \Delta P^2} \quad (2)$$

where \dot{D} is the dose-rate of a grain and $\Delta\dot{D}$ is the associated 1σ uncertainty; \dot{D}_{inf} is the infinite matrix dose-rate derived from the K, Th, U concentrations multiplied by the

corresponding conversion factors, $\Delta\dot{D}_{moist}$ is the moisture content uncertainty and ΔP is the porosity error. For $\Delta\dot{D}_{moist}$, the maximum value of χ (the ratio of effective mass absorption of water versus sediment; Table 4) are included in Zimmerman's (1971) equation:

$$\Delta\dot{D}_{moist} = \chi \cdot \dot{D}_{dry} \cdot \Delta Wf / (\chi \cdot Wf - (\chi - 1))^2$$

where Wf is the ratio between the wet sediment mass and the dry sediment mass and \dot{D}_{moist} and \dot{D}_{dry} are the dose rates of the wet and dry sediment respectively. Simulations using the DosiVox software are constrained by the following approximations: (i) deposits are composed of (mono-mineral) grains of quartz, and these quartz grains represent most of the sample's silica and (ii) all other sample components including radioactivity hotspots (e.g., grains of zircon and K-feldspar) are homogeneously distributed in the matrix.

2.5 Comparing the approaches

To facilitate comparison between the calculation and simulation approaches some elements that are part of standard dose-rate estimations had to be simplified or even omitted: for the six LV samples the radioactivity was assumed to be exclusively derived from the matrix, hence external, with no contribution from cosmic and grain-internal radioactivity. Furthermore, alpha doses-rates were not corrected for alpha efficiency. In terms of grain size, comparability was ascertained by selecting the grain sizes 11.7 μm for LV100 and 94 μm for all other LV samples. For the heterogeneous Mas d'Azil sample, mass-weighted average values of the different layers (Table S1) were employed in DRAC. Because uncertainty estimation is key when comparing the approaches, they are discussed in detail in section 3.3.

3. Results and Discussion

3.1 Dose-rate comparison

The results are displayed in Figs 1, 2 and 3 and listed in Table 2. The dose-rates delivered by the two web-based calculators are identical within 1σ uncertainty, whilst the spreadsheet derived values are systematically higher than the web-based results (Table 3). This is because different moisture attenuation factors are used for the beta dose-rate: In the spreadsheet Guerin and Mercier's (2012) value of 1.19 is used whereas in DRAC the 1.25 value of Zimmerman (1971) is used. Thus, the three calculator methods yield consistent values for beta and gamma dose-rates. This confirms the findings of Durcan et al. (2015, their Figure 5) who show that dose-rate results are consistent, where fixed

conversion and attenuation factors are used. There are some subtle differences in uncertainty estimates calculated by the spreadsheet, DRAC and DRc, but these show no clear pattern (Table 2 and 3). These are likely due to the use of different algorithms between calculators. DosiVox confirm the results of the three dose-rate calculators within a 2σ uncertainty (Fig. 1-3). The simulations reveal a grain-size dependence of dose rate, where the alpha dose-rate decreases with increasing grain size, the beta dose-rate increases with increasing grain size up to $94\ \mu\text{m}$ and decreases for larger grains (Figs. 1 and 2). The grain-size dependence is also seen in the gamma dose-rates, but to a lesser extent. This confirms earlier studies which suggest charge build-up and attenuation is controlled by the irradiated grain-size fraction (Goedicke, 2007; Armitage and Bailey, 2005; Wintle and Aitken, 1977).

3.2 Dose-rate sensitivity to sediment properties

Porosity, bulk density and grain-size distribution are sample-specific properties that are currently not considered in the calculators. To test the impact of grain-size distribution and porosity on dose-rate determination, four sensitivity experiments were run using sample LV100 (denoted as LV100-A,-B,-C,-D). Grain-size distribution was varied using a peak at $6\ \mu\text{m}$ for the $2\text{-}23\ \mu\text{m}$ grain-size fraction (LV100-A, clay to silt fraction) and a peak at $375\ \mu\text{m}$ for the $188\text{-}750\ \mu\text{m}$ grain-size fraction (LV100-B, fine to coarse sand fraction). Porosity was set to 70 % (LV100-C) and to 30 % (LV100-D). All other parameters were kept constant. Results of these experiments are shown in Fig. 4 a and b, where the simulated alpha and beta dose-rates are plotted against grain size. The plots reveal that for small and large grains (e.g., $6\ \mu\text{m}$ and $350\ \mu\text{m}$) the alpha dose-rate remains constant; the beta dose-rate decreases for sand and increases for silt by around 8%. With porosity of 30% and increasing grain size alpha dose-rate increases by around 10% and beta dose-rate decreases by around 10%. With porosity of 70% and increasing grain size, the alpha dose-rate decreases by around 50% and the beta dose-rate increases by around 40%. We note therefore that the effect of porosity on dose rate is dependent on grain size and that porosity affects the accuracy of alpha and beta dose-rates more significantly than grain size. Certainly, these effects are smaller for the total dose-rate, once the alpha dose-rate has been corrected for efficiency. Furthermore, if the effect of porosity on dose rate is grain-size dependent, so should be the effect of moisture on the beta dose-rate. The χ value resulting from each beta-simulation was therefore recorded but the differences between grain-size classes were

small and subject to stochastic uncertainty. The average χ value for beta radiation, typically close to the 100 μm grain-size χ value, was therefore calculated for each sample (Table 4). Inevitably, this average χ value is different to the factor calculated by Zimmerman (1971), because Zimmerman determined it for small-sized objects in a homogeneous SiO_2 matrix. For all LV samples our average χ value for beta radiation is smaller than Zimmerman's value (Table 4) regardless the amount of water in the sediment; only the degree of discrepancy varies with water content. This suggests the use of the factor published by Nathan and Mauz (2008) and Guerin and Mercier (2012) for standard dose-rate calculations.

3.3 Uncertainty of the simulated dose rate

The uncertainties of the simulation results are relatively large compared to those obtained from the calculators (Table 2). Four reasons seem likely: first, for alpha and beta simulations porosity and grain-size distribution are important sources of uncertainty (Fig. 4). Our sensitivity tests indicate 22 % difference for the alpha and 16 % difference for the beta dose-rates when porosity is increased or decreased by 40% of the initial porosity of the sample (for equal grain size). Assuming a 5 % uncertainty on the porosity value and a linear relationship between dose rate and porosity (note that this requires confirmation by further simulations), an uncertainty of 3% and 2 % for the alpha and beta dose-rates respectively is assumed. Moreover, changing the average grain size by an order of magnitude (a tenth of the original average fine-silt grain size and a factor of 10 of the original coarse sand grain size) leads to a maximum variation of 12% and 2 % of the alpha and beta dose-rate respectively. Thus, the error resulting from grain-size distribution has an effect, albeit minor, on the overall alpha and beta dose-rate uncertainties. The same should be the case for the gamma dose-rate, because it is less sensitive to geometric effects. Secondly, for gamma simulations counting statistics are important because the number of ionization events decreases with decreasing grain size. Also, gamma rays transfer their energy heterogeneously along their trajectory which becomes important when the dosimeter is smaller than the radiation range. For example, the data presented here originate from simulation of $5 \cdot 10^8$ gamma-rays (approx. one month simulation time) and yet, high statistical dispersion (up to 50 %) is evident for those samples that required simulation of a large number of grains. As a consequence, simulation times of several days up to several weeks may be required to obtain statistically representative results for the gamma dose-rate. Thirdly, the Monte-Carlo simulation includes more parameters, hence more sources of uncertainty, than the

calculators. Fourthly, radionuclide uncertainties are regarded as being equal, hence added linearly (see equation 2 in section 2.4) because systematic and random errors are not obtained separately from the techniques used for determining radionuclide concentrations.

Overall, the results of this study suggest that the dominant contributors to the DosiVox dose-rate uncertainty are the statistical dispersion of the Monte Carlo calculation and the radionuclide uncertainties.

3.4 Dose-rate estimates of the heterogeneous sample (Mas d’Azil)

The succession of layers were implemented in the simulation and results for 100 μm grains are shown in Fig. 5 (for data see supplementary information, Table S1). Alpha dose-rates obtained from DosiVox are significantly higher than those obtained from DRAC (Fig. 5a) and beta dose-rates fluctuate around the value obtained from DRAC (Fig. 5b). The uncertainty derived from DRAC does not reflect the large dose-rate variability of the different layers. Thus, when the sedimentary deposit is heterogeneous alpha- and beta dose-rates are spatially variable and the calculator’s dose rate is inaccurate for the alpha- and too precise for the beta dose rate.

4. Conclusions and Recommendations

This study shows that for ‘standard’ samples used in dosimetric dating, dose-rates obtained from the three dose-rate calculators are consistent within uncertainties. This indicates that the commonly used approach is robust, which is perhaps unsurprising because these calculators employ the same or similar factors for energy attenuation, absorption and conversion to dose rates. Differences in dose-rate uncertainties between the three dose-rate calculators are non-systematic and are likely a consequence of subtle differences in the error propagation procedures. That is why it is recommended to use the web-based calculators instead of a bespoke spreadsheet.

Simulations using DosiVox confirm the results of the three dose-rate calculators for the samples and the specific grain-size window (94 μm) used in this study. This, again, confirms the robustness of the commonly used approach which is certainly surprising because physical and chemical sediment properties should affect the dose rate. Notwithstanding, DosiVox simulation is a unique diagnostic tool, beneficial in particular for samples originating from complex depositional environments for which we note dose-rate differences between simulation and calculation.

The total dose-rate uncertainty is small when calculating dose rates, but is relatively large for DosiVox simulations because DosiVox includes more parameters and additional contributions from counting statistics. This means that radiation-field modelling should be undertaken for samples originating from complex sedimentary environments because the uncertainty delivered by a calculator may be underestimated.

Appendix: Supplementary data

The raw data of individual layers of the heterogeneous sample “Mas d’Azil” is given in supplementary data (Table S1). Grain-size distribution data are provided in Table S2.

Acknowledgements:

GEK acknowledges support from Swiss National Science Foundation grant number PZ00P2-167960. We thank the two anonymous reviewers for their thoughts and comments.

References:

- Adamiec, G., Aitken, M.J., 1998. Dose-rate conversion factors: update. *Ancient TL*, 16: 37-46.
- Aitken, M. J., 1985. *Thermoluminescence dating*, Academic Press, London.
- Armitage, S.J., Bailey, R.M., 2005. The measured dependence of laboratory beta dose rates on sample grain size. *Radiat. Meas.*, 39: 123-127.
- Bell, W. T., 1979. Attenuation factors for the absorbed radiation dose in quartz inclusions for thermoluminescence dating, *Ancient TL*, 8, 2-13.
- Brennan, B.J., Lyons, R.G., Phillips, S.W., 1991. Attenuation of alpha particle track dose for spherical grains. *Int. J. Radiat. Appl. Instrum. Part D. Nucl. Tracks Radiat. Meas.*, 18: 249-253.
- Brennan, B. J., 2003. Beta doses to spherical grains, *Radiation Measurements*, 37(4–5), 299-303.
- Durcan, J.A., King, G.E., Duller, G.A.T., 2015. DRAC: Dose rate and age calculator for trapped charge dating. *Quaternary Geochronology*, 28: 54-61.
- Goedicke, S., 2007. Calibration of a $^{90}\text{Sr}/^{90}\text{Y}$ -source for luminescence dating using OSL. *Radiat. Meas.*, 42: 1427-1431.
- Guérin, G., Mercier, N., Adamiec, G., 2011a. Dose-rate conversion factors: update. *Ancient TL*, 29: 5-8.
- Guérin, G., 2011b. Modélisation et simulations numériques des effets dosimétriques dans les sédiments quaternaires: application aux méthodes de datation par luminescence. Doctoral thesis in Physique des archéomatériaux, Bordeaux, université Michel de Montaigne Bordeaux3, 242p.
- Guérin, G., Mercier, N., Nathan, R., Adamiec, C., Lefrais, Y., 2012. On the use of the infinite matrix assumption and associated concepts: a critical review. *Radiat. Meas.*, 47: 778-785.
- Guérin, G., Mercier, N., 2012. Preliminary insight into dose deposition processes in sedimentary media on a scale of single grains: Monte Carlo modelling of the effect of water on the gamma dose rate. *Radiation Measurements* 47: 541-547.
- Hipondoka, M.H.T., Mauz, B., Packman, S., Bloemendal, J., Chiverrell, R., Kempf, J. Sand ridge dynamics and the Holocene evolution of the Etosha Pan (Namibia). *Geomorphology* 204, 553-563.

- Lang, A., Lindauer, S., Kuhn, R., Wagner, G.A., 1996. Procedures used for optically and infrared stimulated luminescence dating of sediments in Heidelberg. *Ancient TL*, 14, 7-11.
- Liritzis, I., Stamoulis, K., Papachristodoulou, C., Ioannides, K., 2013. A re-evaluation of radiation dose-rate conversion factors. *Mediterr. Archaeol. Archaeom.* 13, 1-15.
- Kreutzer, S., Dietze, M., Burow, C. (2017). `use_DRAC()`: Use DRAC to calculate dose rate data. Function version 0.1.1. In: Kreutzer, S., Dietze, M., Burow, C., Fuchs, M.C., Schmidt, C., Fischer, M., Friedrich, J. (2017). *Luminescence: Comprehensive Luminescence Dating Data Analysis*. R package version 0.7.5. <https://CRAN.R-project.org/package=Luminescence>
- Martin, L., Incerti, S., Mercier, N., 2015a. DosiVox: Implementing Geant 4-based software for dosimetry simulations relevant to luminescence and ESR dating techniques. *Ancient TL*, 33(1): 1-10.
- Martin, L., Mercier, N., Incerti, S., Lefrais, Y., Pecheyran, C., Guérin, G., Jarry, M., Bruxelles, L., Bon, F., Pallier, C., 2015b. Dosimetric study of sediments at the beta dose rate scale: Characterization and modelization with the DosiVox software. *Radiation Measurements*, 81: 134-141.
- Mauz, B., Vacchi, M., Green, A., Hoffmann, G., Cooper, A. Beachrock. 2015. A tool for reconstructing relative sea level in the far-field. *Marine Geology* 362, 1-16.
- Mejdahl, V., 1979. Thermoluminescence dating: beta-dose attenuation in quartz grains. *Archaeometry* 21: 61-72.
- Nathan, R. P., Mauz, B., 2008. On the dose-rate estimate of carbonate-rich sediments for trapped charge dating, *Radiation Measurements*, 43, 14-25.
- Prescott, J. R., Stephan, L. G., 1982. The contribution of cosmic radiation to the environmental dose for thermoluminescence dating: latitude, altitude and depth dependences, *PACT*, 6, 17-25.
- Prescott, J. R., Hutton, J. T., 1988. Cosmic ray and gamma ray dosimetry for TL and ESR, *International Journal of Radiation Applications and Instrumentation. Part D. Nuclear Tracks and Radiation Measurements*, 14, 223-227.
- Prescott, J. R., Hutton, J. T., 1994. Cosmic ray contributions to dose rates for luminescence and ESR dating: large depths and long-term time variations, *Radiation Measurements*, 23, 497-500.
- Preusser, F., Kasper, K.U., 2001. Comparison of dose rate determination using high resolution gamma spectrometry and inductively coupled plasma-mass spectrometry. *Ancient TL* 19, 19-23.
- Readhead, M. L., 2002a. Absorbed dose fraction for ^{87}Rb β particles, *Ancient TL*, 20, 25-28.
- Readhead, M.L., 2002b. Appendix to “Absorbed dose fraction for ^{87}Rb beta particles”. *Anc. TL* 20, 47
- Roesch, W.C., Attix, F.H., 1968. Basic concepts of dosimetry. In: Attix, F.H., Roesch, W.C., Tochilin, E. (Eds.), *Radiation Dosimetry*, Academic Press, New York.
- Tsakalos, E., Christodoulakis, J., and Charalambous, L., 2016. The Dose Rate Calculator (DRc) for Luminescence and ESR Dating – a Java Application for Dose Rate and Age Determination. *Archaeometry*, 58: 347-352.
- Wentworth, C.K., 1922. A Scale of Grade and Class Terms for Clastic Sediments. *The Journal of Geology*.
- Wintle, A.G., Aitken, M.J., 1977. Absorbed dose from a beta source as shown by thermoluminescence dosimetry, *Int. J. Appl. Radiat. Isot.*, 28: 625-627.
- Wu, W., Wang, S.S.Y., 2006. Formulas for Sediment Porosity and Settling Velocity. *Journal of Hydraulic Engineering*, 132(8): 858-862.
- Zimmerman, D. W., 1971. Thermoluminescent dating using fine grains from pottery. *Archaeometry*, 13: 29-52.

Figure Captions

Figure 1. The alpha dose-rate of LV100. The grain-size fraction of 4-11 μm is used in the three calculators. No alpha-efficiency correction was applied. Uncertainties are depicted at the 1σ level.

Figure 2. Beta dose-rates of all LV samples (note y-axis log scale). For clarity, uncertainties (1σ) are depicted for the 94 μm grain size only. Corresponding data are listed in Table 3.

Figure 3. Gamma dose-rates of all LV samples (note y-axis log scale). For clarity, uncertainties (1σ) are depicted for the 94 μm grain size only. Corresponding data are listed in Table 3.

Figure 4. Results of DosiVox sensitivity test using the data of LV100: (a) Alpha dose-rate and (b) beta dose-rate. LV100-A (clay to silt fraction) and LV100-B (fine to coarse sand fraction) denote two different grain-size fractions (see text for details). LV100-C and LV100-D denote two different porosities (see text for details). For clarity, error bars (estimated to be $\sim 5\%$ at 1σ) are not shown.

Figure 5. Results for the heterogeneous sample (Mas d’Azil): (a) alpha and (b) beta dose-rate. The simulation used the 100 μm grains. DRAC results based on mass-weighted average values of the different layers are displayed for comparison. For clarity, error bars for the DosiVox results (estimated to be $\sim 5\%$ at 1σ) are not shown.

Tables

Table 1. Samples used in this study. For each sample, lab code, water content (H_2O % dry weight of field moisture at time of sampling; error term accounts for presumed moisture fluctuation during burial), U and Th concentration, K weight %, grain-size range of the dosimeter, chemical composition (% dry weight), pore volume, calculated quartz concentration and sample description are listed. A reference is listed where sample is published. For Mas d’Azil mass-weighted average values of the layers are listed.

Table 2. Beta-, gamma- and total dose-rates and associated 1σ uncertainties resulting from calculation (Spreadsheet, DRAC, DRc) and simulation (DosiVox). All data are derived from the 94 μm grain size except for LV100 for which 11.7 μm was used. The uncertainties obtained from DosiVox are higher than those obtained from DRAC: they are 1060% higher for beta dose rate and up to around 140% higher for gamma dose rate.

Table 3. Total (beta and gamma) dose-rates normalized to the values obtained from DRAC and their 1σ uncertainty. The alpha component was not included in the total-dose rate.

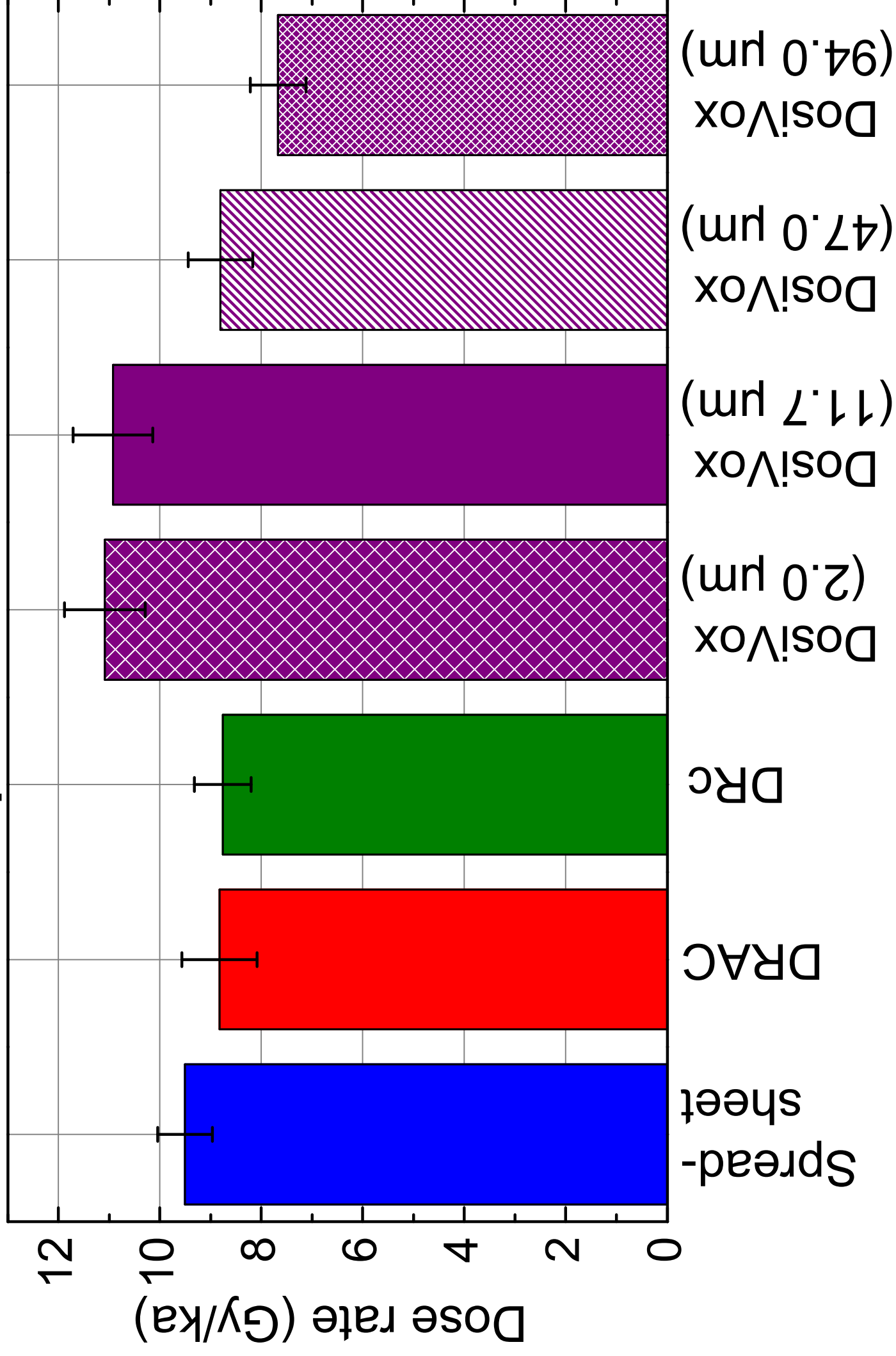
Table 4. Average and maximum χ factor for beta radiation calculated according to each sample’s grain-size distribution and moisture content. The deviation from the

466 Zimmerman Factor (1.25) is listed. For LV100 alpha radiation is also considered.
467 Grain-size distribution is here summarised as median. For grain-size data see Table
468 S2.

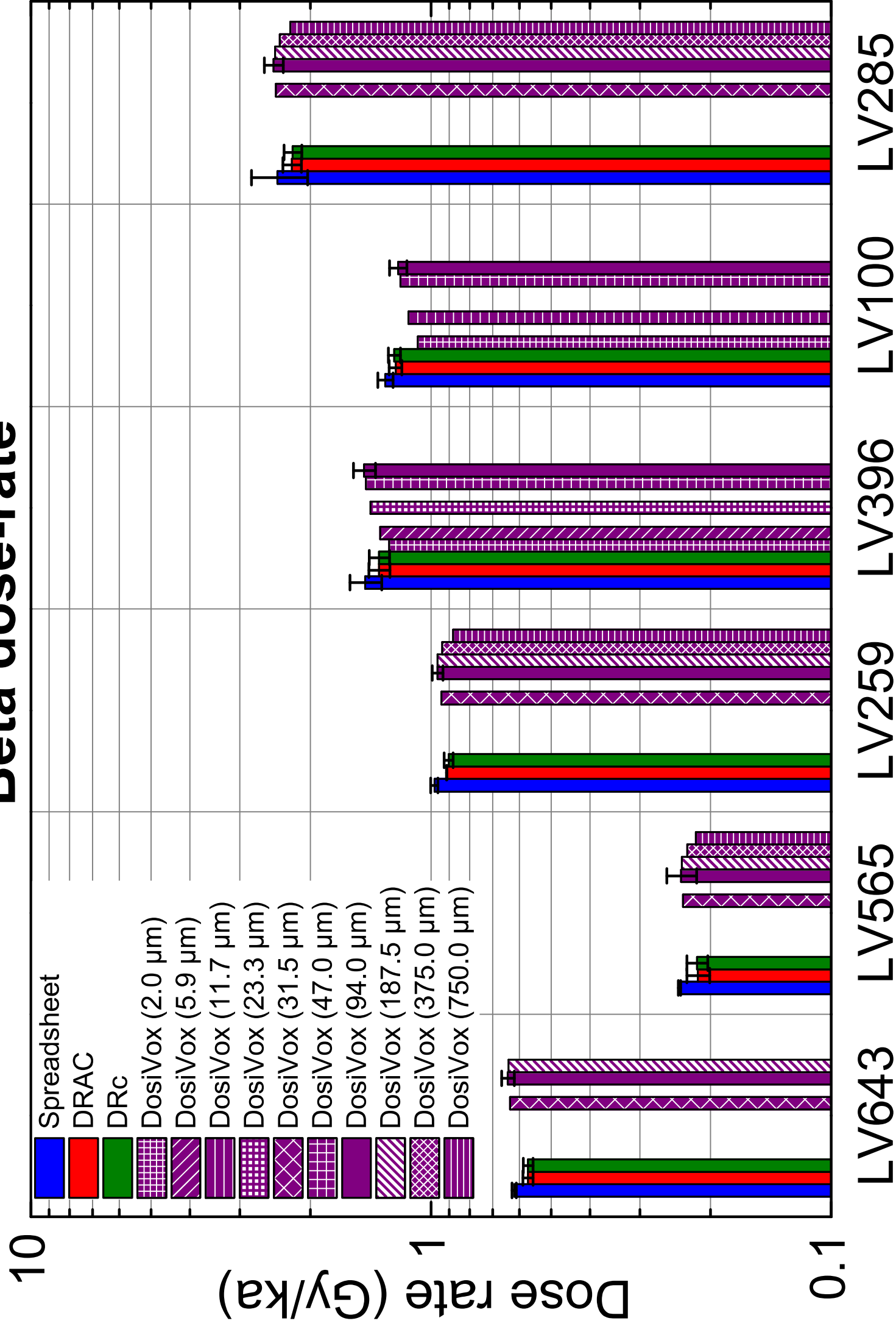
469 Table S1. Analytical data of the individual layers of the heterogeneous sample Mas
470 d'Azil used for the simulations.

471 Table S2. Grain-size distribution of samples used in this study following the Wentworth
472 (1922) classification. The mean of class as used for DosiVox simulations is also
473 listed.

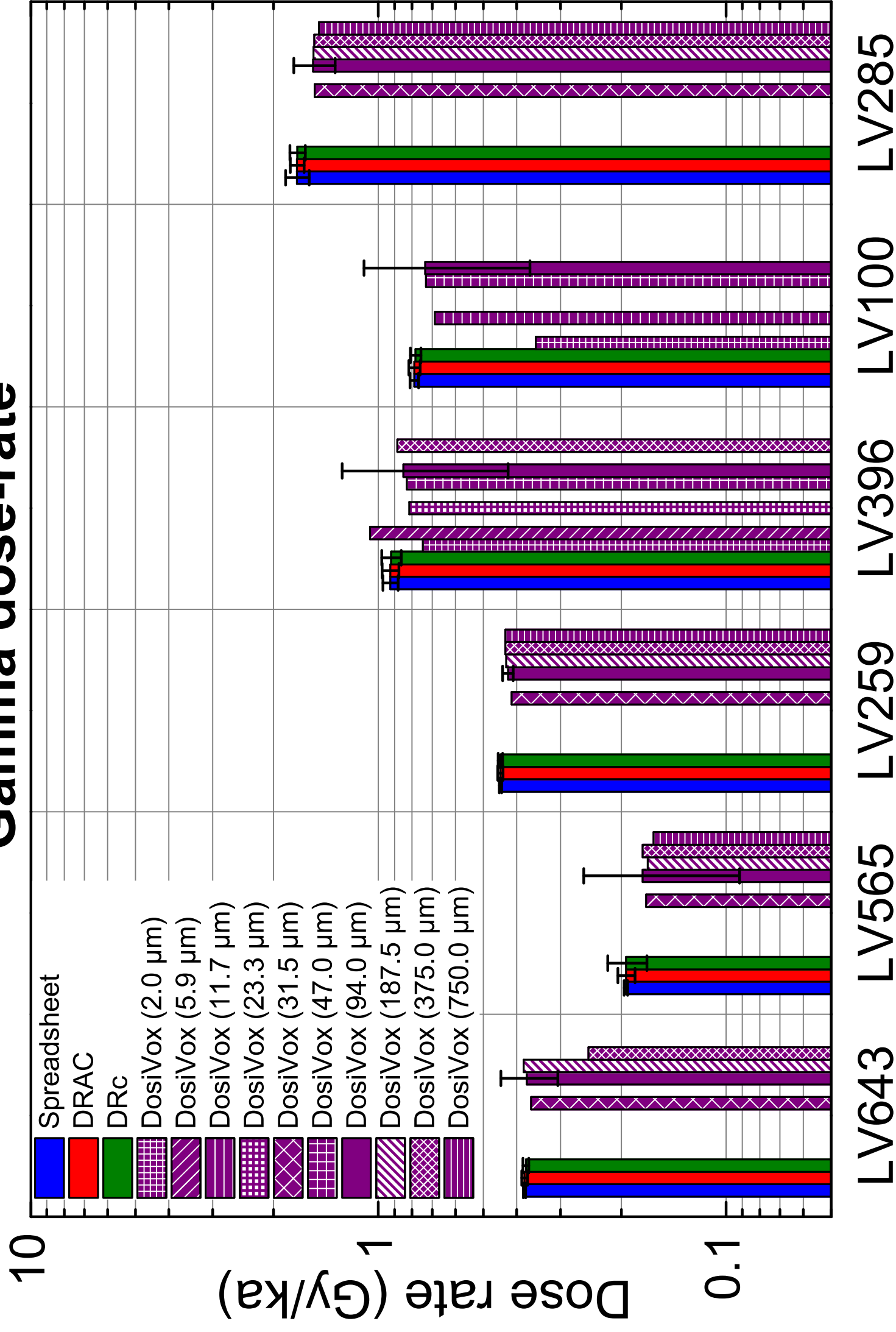
Alpha dose-rate



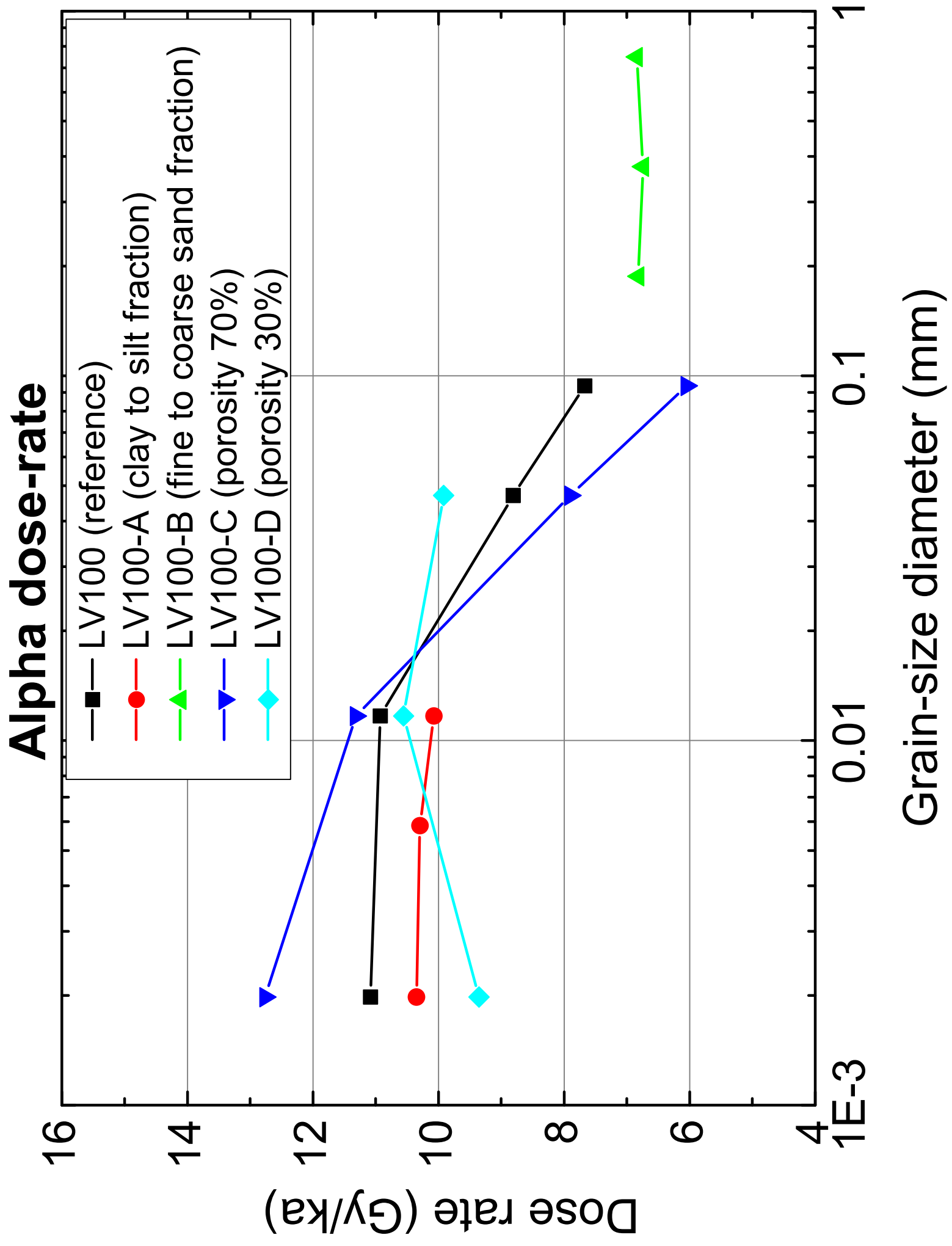
Beta dose-rate



Gamma dose-rate

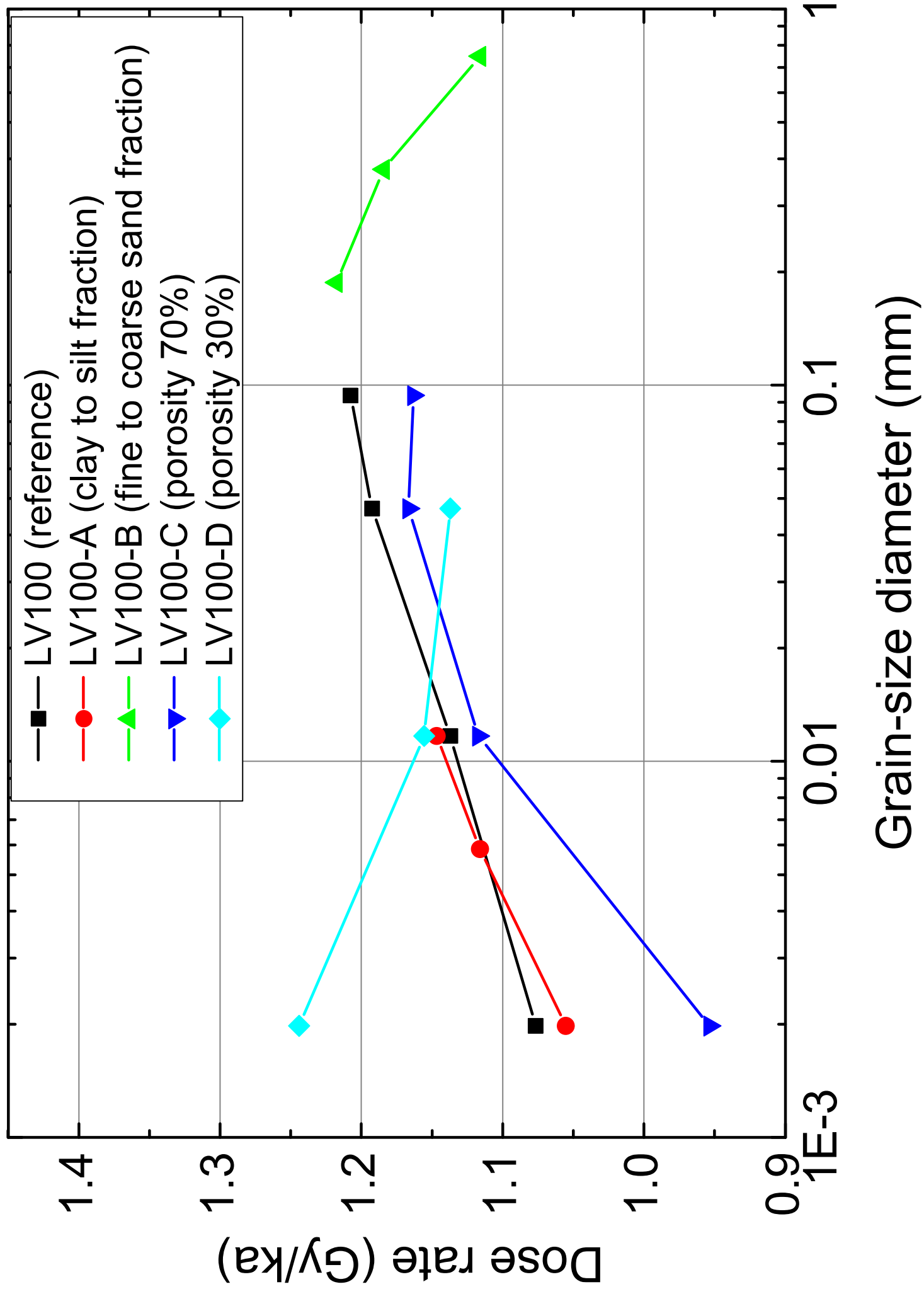


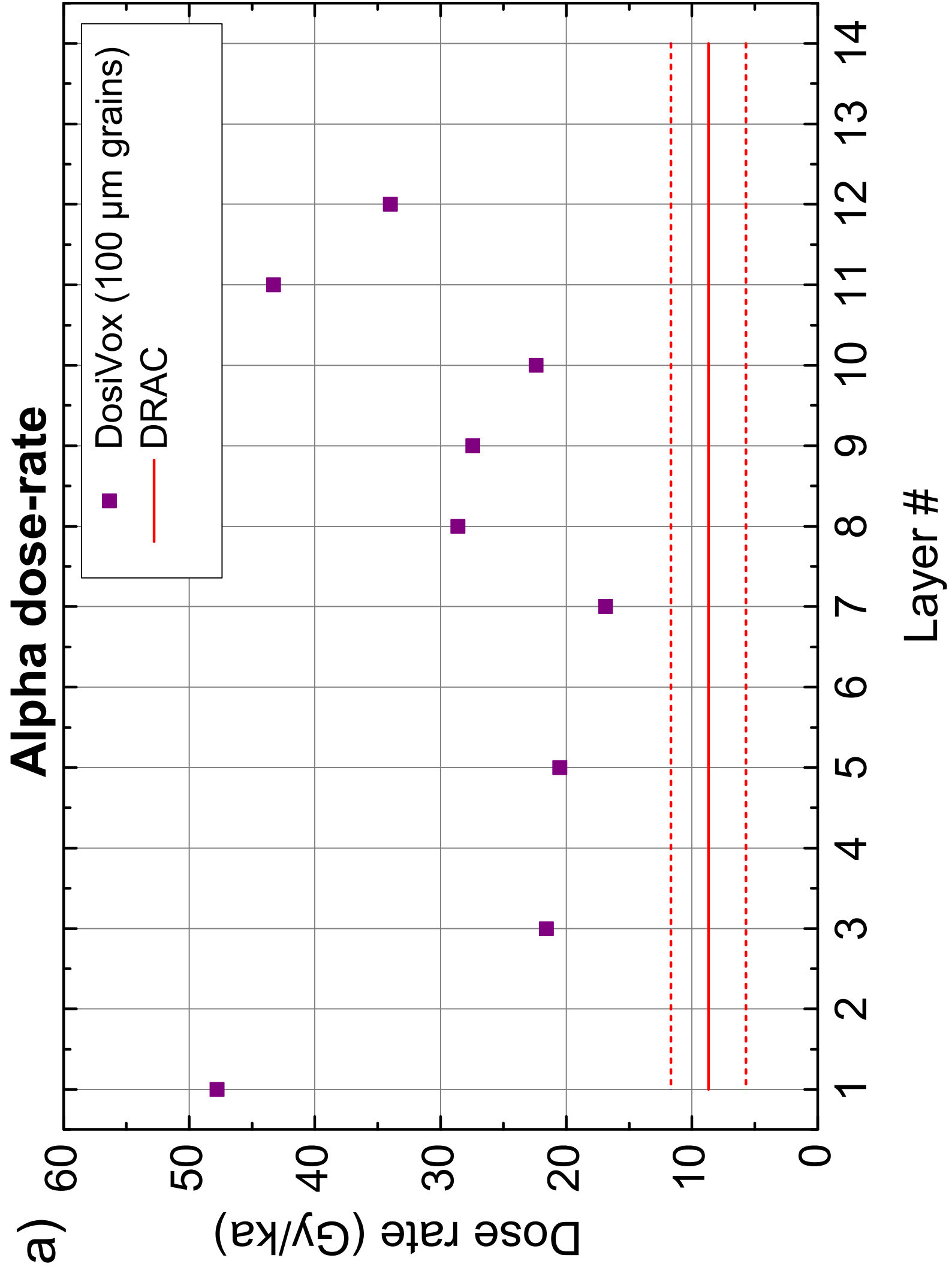
a)



b)

Beta dose-rate





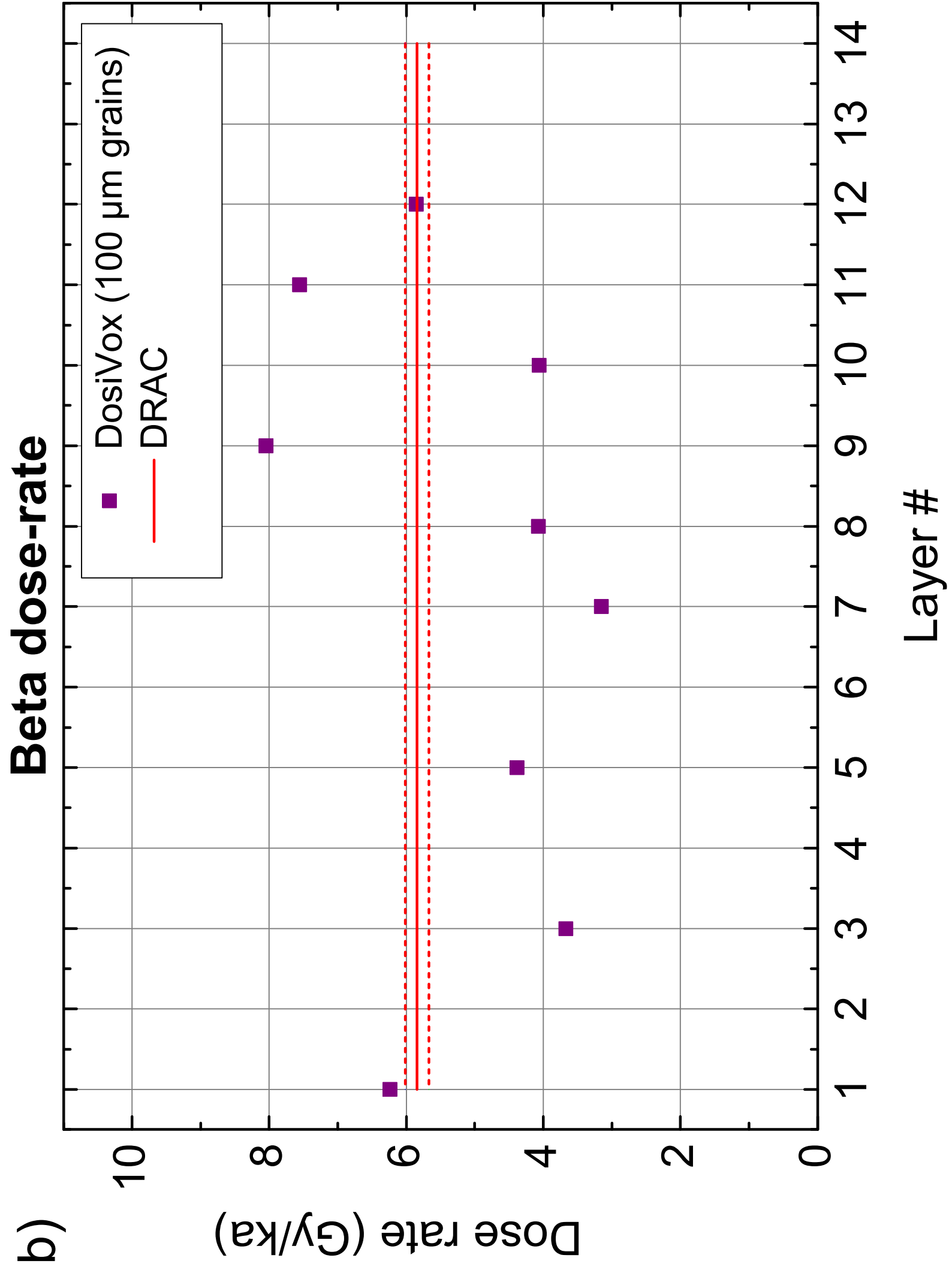


Table 1

Sample	H ₂ O (%)	U (ppm) Th (ppm) K (%)	Dosimeter grain-size (µm)	SiO ₂ Al ₂ O ₃ Ca/MgCO ₃ (%)	KAISi ₃ O ₈ Fe ₂ O ₃ NaCl K ₂ O (%)	Sediment porosity (%)	Max. proportion of quartz for simulation (%)	Sample description
LV643	20±1	1.14±0.03 3.66±0.09 0.66±0.02	100-200	90.5 1.2 -/-	8.0 0.3 - -	45	49.9	Loose sand, fluctuating water level, mostly water- saturated during burial, tropical environment (unpublished)
LV565	3±2	0.80±0.09 1.71±0.05 0.12±0.01	100-200	5.2 0.5 93.1/-	0.9 0.3 - -	42	3.0	Cemented sand, ~90 % of sample volume is carbonate, arid environment (Mauz et al., 2015)
LV259	0	1.00±0.03 1.82±0.05 0.99±0.02	100-200	61.3 2.1 29.4/-	6.6 0.6 -	44	34.5	Loose quartz sand, arid environment (unpublished)
LV396	15±5	3.60±0.20 7.30±0.27 1.33±0.03	100-200	40.1 4.3 36.5/-	9.2 0.8 9.1 -	48	15.7	Loose sand, significant secular disequilibrium due to ²²⁶ Ra uptake, semi- arid environment (Hipondoka et al., 2013)

LV100	17.5±2.5	2.50±0.20 8.00±0.20 1.14±0.03	4-11	59.5 6.1 21.3/5.3	4.8 1.6 1.4 -	51	29.2	Loose silt, loess, temperate environment ("Nussi"; (Preusser and Kasper, 2001)
LV285	4±4	3.87±0.10 18.28±0.35 1.95±0.05	100-200	58.3 9.0 5.8/-	15.0 11.9 - -	44	32.6	Sand and gravel, tropical environment (unpublished)
Mas d'Azil	15±6	6.24±0.31 30.87±0.93 5.52±0.17	100-200	64.2 17.3 -	- 12.2 - 6.2	-	-	Archaeological deposit: succession of laterally homogeneous mm-thick layers of varying composition (Martin et al., 2015b)

Table 2

Sample	Spreadsheet			DRAC program			DRc program			DosiVox		
	Beta	Gamma	Beta+ Gamma	Beta	Gamma	Beta+ Gamma	Beta	Gamma	Beta+ Gamma	Beta	Gamma	Beta+ Gamma
LV643	0.619±0.008	0.380±0.003	0.999±0.008	0.572±0.017	0.380±0.007	0.952±0.018	0.572±0.016	0.377±0.007	0.949±0.017	0.641±0.023	0.375±0.070	1.016±0.074
LV565	0.239±0.001	0.194±0.002	0.433±0.003	0.215±0.014	0.194±0.011	0.409±0.018	0.216±0.013	0.194±0.025	0.410±0.028	0.237±0.020	0.174±0.083	0.411±0.085
LV259	0.980±0.021	0.446±0.003	1.426±0.021	0.913±0.001	0.446±0.008	1.359±0.008	0.902±0.023	0.446±0.007	1.348±0.024	0.962±0.030	0.424±0.015	1.386±0.033
LV396	1.461±0.133	0.925±0.047	2.385±0.141	1.346±0.080	0.925±0.051	2.271±0.095	1.346±0.077	0.919±0.059	2.265±0.097	1.469±0.093	0.847±0.423	2.315±0.433
LV100	1.300±0.056	0.788±0.022	2.088±0.060	1.225±0.045	0.788±0.029	2.013±0.054	1.234±0.043	0.782±0.028	2.016±0.051	1.137±0.057	0.688±0.344	1.825±0.348
LV285	2.417±0.388	1.715±0.134	4.133±0.410	2.223±0.120	1.715±0.079	3.938±0.144	2.213±0.114	1.712±0.088	3.925±0.144	2.471±0.134	1.543±0.210	4.014±0.249

Table 3

Sample	Total Dose Rate		
	Spread-sheet	DRc program	DosiVox
LV643	1.05±0.01	1.00±0.02	1.07±0.07
LV565	1.06±0.01	1.00±0.07	1.01±0.21
LV259	1.05±0.01	0.99±0.02	1.02±0.02
LV396	1.05±0.06	1.00±0.04	1.02±0.19
LV100	1.04±0.03	1.00±0.03	0.91±0.19
LV285	1.05±0.10	1.00±0.04	1.02±0.06

Table 4

Sample	Grain size (median; μm)	Moisture content (% of dry mass)	Average χ factor	Deviation from the 1.25 Zimmerman Factor (%)	Maximum χ factor
LV 259	224.0	0	1.07	-14	1.10
LV 285	193.4	4 \pm 4	1.07	-14	1.15
LV 396	94.0	15 \pm 5	1.10	-12	1.16
LV 565	326.7	3 \pm 2	0.99	-21	1.21
LV 643	174.2	20 \pm 1	1.21	-3	1.23
LV 100 (β)	47.0	17.5 \pm 2.5	1.13	-10	1.15
LV 100 (α)	47.0	17.5 \pm 2.5	1.36	-	1.88

Table S2.

Grain-Size Class (Wentworth, 1922)	DosiVox Mean of Class (μm)	LV259 Grain Size (%)	LV285 Grain Size (%)	LV565 Grain Size (%)	LV643 Grain Size (%)	LV396 Grain Size (%)	LV100 Grain Size (%)
Very Coarse Sand	1500	0.2	0.5	3.1	0.7	28.0	0.7
Coarse Sand	750	11.8	17.0	29.8	5.2	-	7.9
Medium Sand	375	33.4	25.6	24.4	10.4	44.0	58.9
Fine Sand	187.5	31.0	16.9	14.4	69.3	7.0	-
Very Fine Sand	94.0	20.9	9.0	9.3	12.4	-	-
Silt and Clay	31.5	2.7	31.0	19.0	2.0	5.0	23.5